ChemComm
Chemical Communications

Accepted Manuscript

This article can be cited before page numbers have been issued, to do this please use: Z. Mengrani, H. Yu, W. Hong, D. Di Tommaso and M. Palma, *Chem. Commun.*, 2026, DOI: 10.1039/D6CC02075E.

ROYAL SOCIETY OF CHEMISTRY

rsc.li/chemcomm

ChemComm

View Article Online
DOI: 10.1039/D6CC02075E

COMMUNICATION

Templated Assembly of Metal Nanoparticles on DNA–SWCNT Hybrids Towards Optoelectronic Tunability

Received 00th January 20xx,
eAccepted 00th January 20xx

DOI: 10.1039/x0xx00000x

Zechariah Mengrani,[a,†] Houlin Yu, [a,†] Weiying Hong,[a] Devis Di Tommaso *,[a] and Matteo Palma *,[a]

DNA is a programmable scaffold for the assembly of low-dimensional heterostructures. Here, we report the formation of 0D-1D nanohybrds via two distinct strategies, utilising DNA as a template and a linker moiety in the controlled assembly of metal sulfide nanoparticles onto single-walled carbon nanotubes.

Integrating low-dimensional materials into functional heterostructures offers a powerful strategy for designing nanomaterials that combine two or more distinct components, in a structure with enhanced or synergistic properties.[1] Single-walled carbon nanotubes (SWCNTs) are promising 1D building blocks and scaffolds for this, due to their physical, chemical, and mechanical properties,[2-4] and high charge carrier mobility that can facilitate charge transfer at interfaces.[5,6] Synergistically combining SWCNTs with metal nanoparticles (NPs) for example could enable optoelectronic tunable 1D-0D hybrids.[5,7]

In this context, controlling the interface between the two materials, in terms of spatial separation and chemical linkage, is crucial as these influence the heterostructure's optoelectronic properties, [8] governing key processes such as photon absorption and charge transfer.[9] Various methods have been developed to form nanohybrids of SWCNTs with NPs, including covalent functionalisation,[10,11] non-covalent modifications,[12,13] including via moieties that can π-π stack onto the SWCNTs.[14-15] These approaches however, present limitations. Covalent functionalisation can disrupt the intrinsic electronic properties of SWCNTs,[16] while bridging moieties may introduce interfacial barriers hindering charge transfer. Moreover, most methods result in indiscriminate loading of NPs onto the SWCNTs.[17–19]

DNA has emerged as a useful material for the non-covalent functionalisation of SWCNTs, by helically wrapping the nanotubes through the interaction of DNA nucleobases via the π-conjugated carbon surface, via π-π stacking, with high stability and chiral selectivity.[20] This enables high solution dispersibility while preserving nanotubes intrinsic features. Moreover, DNA can further act as a programmable linker[21–23] and scaffold.[24-27] However, despite its potential, DNA-mediated seeding of NPs onto SWCNTs has been only sparsely explored, [25,28] and its influence on the morphology of the hybrids and their optoelectronic properties remains largely uncharacterised.

Here, we employ DNA as a template to grow PbS, CdS, and Ag_2S NPs onto SWCNTs using two complementary strategies (Scheme 1): (i) seeding metal cations onto short DNA strands that hybridise to the DNA wrapping the SWCNT, [26,27] producing predominantly single-NP attachment; (ii) in-situ seeding onto the DNA wrapping the SWCNT,[25] producing a denser, nanoparticle decoration along the tube. In the DNA-hybridisation route, short DNA strands complementary to the wrapping strand of the SWCNT were seeded with metal precursors (e.g., $Pb(NO_3)_2$, $Cd(NO_3)_2$). These seeded short strands then hybridise—by design—with a section of the wrapping strand of the SWCNT, before Na_2S addition for nanoparticles growth.[24] Depending on the metal ion used, the binding can occur either on the phosphate backbone of the DNA, on the nucleobases, or on both sites via coulomb and coordinate interactions.[29] Given the thermodynamic strength of the duplex formation between complementary strands, hybridisation is expected to proceed even in the presence of coordinated metal ions: metal ion-associated oligonucleotides have been shown to retain hybridisation capability.[26,27] In contrast, the in-situ seeding method involves introducing metal precursors into the DNA-wrapped SWCNTs solutions prior to Na_2S addition, enabling NPs nucleation and growth directly on the DNA-wrapped nanotube.[25] A $(GT)_{20}$ sequence was employed as previously reported;[25] all other DNA sequences used in this study were designed specifically for this work. [See the supporting information (SI) for the experimental details of both methodologies]. The nanohybrids were characterised and compared using atomic force microscopy (AFM), UV-Vis, Raman, and photoluminescence (PL) spectroscopy.

We employed (6,5) chirality-enriched SWCNTs wrapped with single-stranded DNA (see the SI) due to their distinct excitonic transitions and to ensure optical features correspond to a single species. Each metal sulfide NP (PbS, CdS, Ag_2S) was synthesized independently using single-metal precursor solutions under rigorously separated conditions. Sulfide addition under these

[a] *Department of Chemistry, School of Physical and Chemical Sciences, Queen Mary University of London, Mile End Road, London E1 4NS, United Kingdom*

† These authors contributed equally

Supplementary Information available: [details of any supplementary information available should be included here]. See DOI: 10.1039/x0xx00000x

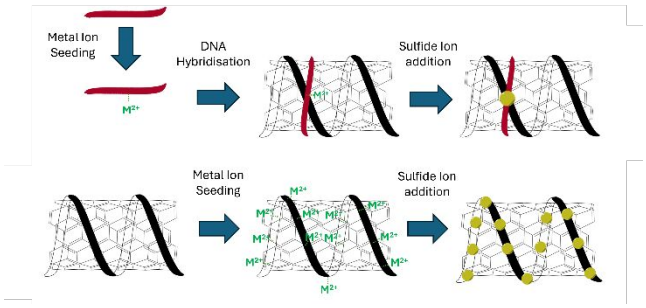

Scheme 1: Strategies for seeding metal NPs on DNA–SWCNT. (i) DNA hybridisation method: short DNA strands pre-seeded with metal precursors hybridise with the DNA wrapping the SWCNT, enabling site-specific nanoparticle attachment. (ii) In-situ seeding method: metal precursors are introduced directly into DNA–SWCNT solutions, leading to in-situ NPs nucleation and dense decoration along the nanotube surface.

conditions leads to the formation of the corresponding metal sulfide.[24] No mixed-metal systems were present at any stage of synthesis. AFM was used to identify the successful formation of CNT-NP nanohybrids, once cast from solution on muscovite mica surfaces, assessing the spatial distribution of metal-sulfide NPs on the DNA-wrapped SWCNTs. Figure 1a shows a representative topographical AFM image of heterostructures formed by the DNA-hybridisation assembly strategy (i), while Figure 1b shows the in-situ growth methodology (ii). The DNA hybridisation method leads to isolated NPs attachment, where single NPs can be seen to bind to one SWCNT, with average sizes of PbS: 5.6±1.5 nm; CdS: 4.5±1.5 nm; and Ag_2S: 6.9±2.8 nm (Figure S1-3). The yield of formation of nanohybrids, defined as the number of CNTs displaying a NP, varies between metal systems; AFM revealed it to be 39% for PbS-, 25% for CdS-, and 37% for Ag_2S-CNTs. This indicates that duplex formation is preserved and yield differences arise from metal-dependent nucleation behaviour rather than inhibited hybridization.

By contrast, the CNT-NP hybrids assembled by the in-situ method (Figure 1b) display a bead-on-a-string morphology of NPs along the SWCNTs. Ag_2S displays slightly more clustered distributions compared to PbS and CdS. Average sizes were found to be 4.3±1.7 nm for PbS, 3.76±1 nm for CdS, and 4.9±2.8 nm for Ag_2S. The yield of formation was 26% for PbS-CNTs, 31% for CdS-CNTs, and 22% for Ag_2S-CNTs (Figure S1-3). The NP density along the SWCNTs produced by this method ranges from 1 to 10 NPs per 500 nm CNT, with a typical value of ~4–7 NPs (Figure S4). Control experiments employing non-complementary strands and preformed nanoparticles confirmed the role of duplex-mediated templating, assessing nonspecific adsorption: nanohybrid formation does not occur without complementary strands (Figure S6), and in-situ seeding is required to form uniformly distributed nanohybrids (Fig. S6).

The distinct morphologies and heights of the NPs seen across the two methods can be attributed to differences in the functionalisation route. Variation in the height (Figure S7) can arise from the number of nucleation sites. It is reasonable to assume that following the in-situ method, there is a higher nucleation site density compared with the DNA hybridisation methodology. A high density of nucleation sites likely leads to competition from precursors and limited growth of individual particles, resulting in smaller average sizes.[30] Indeed, in the DNA hybridisation approach, the metal ion seeding is localised on the short complementary strand before salt addition for growth, resulting in lower surface coverage, more isolated connections, and larger NP sizes. Differently, during the in-situ functionalisation, metal ions can pre-associate with the entire SWCNT-wrapping DNA (phosphate backbone). Upon sulfide addition, these ion–DNA complexes act as multi-localised nucleation sites, promoting denser NP formation.

View Article Online DOI: 10.1039/D6CC02075F

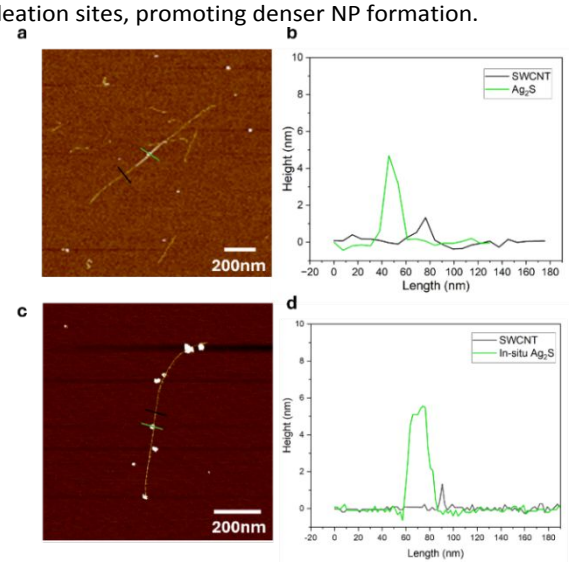

Figure 1: AFM images of DNA-wrapped (6,5) SWCNTs decorated with Ag_2S NPs via two methods. (a) DNA Hybridisation (one-to-one attachment of NPs to SWCNTs), (b) Height profile of the SWCNT and the metal NP. (c) In-situ method (approximately 4–7 NPs per 500 nm of SWCNT length as shown in Figure S4), (d) Height profile of the SWCNT and the metal NP.

The difference observed in the particle density and attachment is expected to modulate the electronic coupling between the NPs and SWCNTs, thereby affecting the optical characteristics. In order to investigate this, we performed a series of spectroscopic measurements on all the CNT-NP hybrids. The UV–vis spectra of the various nanohybrids show a peak shifting in the absorption spectra of DNA–SWCNT hybrids upon attachment of the metal sulfide NPs. Figure S5a shows the first excitonic absorption peak (E_{11}) of the enriched (6,5) chirality SWCNTs used here, before (pristine, ~991 nm) and after attachment of PbS, CdS, and Ag_2S NPs through the DNA hybridisation method; Figure S5b shows the corresponding spectra for in-situ NPs growth. The DNA hybridisation method results in shifts of ~1-2 nm for PbS and CdS, and a shift of 5 nm for Ag_2S. For the in-situ method in all cases, the characteristic SWCNT E_{11} absorption peak shifts to a longer wavelength ~3-5 nm (lower energy) upon NP functionalization. This red shift likely reflects electronic coupling between the NPs and SWCNTs. Two key physical mechanisms are known to contribute to these spectral shifts: (i) dielectric screening, where the polarizable environment of the NPs reduces the Coulomb attraction between the electron–hole pair in the SWCNT exciton, thereby lowering the exciton binding energy and the optical gap;[31] (ii) charge-transfer doping, in which the injected or withdrawn charge carriers cause many-body bandgap renormalisation, further lowering the energy of the E_{11} transition.[32] A shift of the E_{11} peak is well-documented in doped or dielectric-shelled

SWCNTs.[31,32] From our findings, we can see that the magnitude of the red shift varies depending on the NP type and most notably attachment method, with in-situ growth resulting in a larger red shift of ~3-4nm compared to the DNA hybridisation method(~1-2nm) for PbS and CdS attachment. For Ag_2S, the magnitude of the shift is the same across the methods (~5 nm). The larger red shifts observed for PbS and CdS can be attributed to the NP loading, as the in-situ functionalisation route promotes a greater density of NPs, likely more intimately coupled onto the nanotubes compared to what the hybridisation strategy produces. In contrast, Ag_2S shows similar shifts for both strategies despite differences in the NP loading. This suggests that the Ag_2S optical transition is less sensitive to differences in nanoparticle coverage or interfacial coupling with the CNT compared to PbS and CdS. The shifts are relatively small in absolute terms for (6,5) SWCNTs, implying that while the bandgap is measurably perturbed, the electronic structure of the carbon nanotubes is likely not drastically altered.[33,34] This likely originates from the NP attachment occurring through non-covalent, non-destructive interactions, hence preserving the intrinsic properties of the SWCNTs.[35]

Raman spectroscopy allowed us to probe the structural and electronic changes induced by NP loading on the SWCNTs.[36] Figure 2a,b displays the G-band of the nanohybrids compared to the pristine SWCNTs, with Figure 2c,d displaying the 2D or G' band. The broadening or shifting of these key peaks is a strong indicator of doping or strain effects on the SWCNTs.[34] When comparing the two methods, the DNA hybridisation leads to a small upshift of ~1-2 cm^{-1} in the G band compared to a strong downshift for the in-situ method of up to 6 cm^{-1} seen for the Ag_2S addition. As neither methodology leads to defect formation in the SWCNTs, it is reasonable to attribute any optical changes to electronic effects. The small upshift in the G-band seen in the DNA hybridisation method can be ascribed to a weak doping effect of the NPs on the SWCNT[37], with a large downshift seen in the in-situ method attributed to a stronger doping of the SWCNTs. The stronger downshift observed for Ag_2S may arise from differences in local NP–SWCNT interactions and structural perturbations stemming from more clustered distributions of NPs on the SWCNT (Figure S3c), in addition to doping effects. No distinct difference in the G' band compared to the other NPs is seen, further supporting this (see below).

The G' band is more sensitive to electronic changes in the system, such as Fermi level shifts.[32] There are no noticeable changes seen in the DNA hybridisation method, with a noticeable red-shifting of ~4-6 cm^{-1} seen in the in-situ method. This can be attributed to electron-induced doping with a red shift in the G' band, generally associated with N-type doping.[38] From these observations, we ascribe the optical modulations predominantly to subtle electronic interactions rather than structural changes of the SWCNTs. To further assess the impact of NPs on the SWCNT properties, we characterised our nanohybrids via PL spectroscopy. Representative spectra selected from multiple independent measurements are shown in Figure 3. The key emission peak for pristine (6,5) SWCNTs corresponds to the E_{11} transition at 994nm.

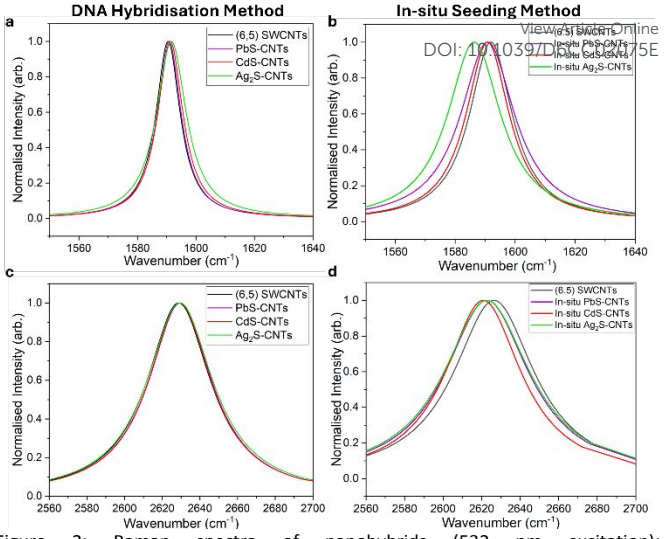

Figure 2: Raman spectra of nanohybrids (532 nm excitation): (a, b) G-band; (c, d) G'-band from (a, c) of nanohybrids via the DNA hybridisation and (b, d) in-situ seeding methods.

Enhancement or quenching refers to relative changes in the measured PL intensity compared to the reference SWCNT sample. For the DNA hybridisation method, we observe a CNT PL intensity enhancement of 8% for PbS and 1% for CdS, but a 13% quenching for Ag_2S-CNT heterostructures (Figure 3a). It is reasonable to assume that in the DNA hybridisation method, metal ions preferentially bind to the DNA scaffold rather than forming metal sulfide nanoparticles. The PL response, therefore, reflects competing contributions from residual metal ions and sparsely formed nanoparticles. Pb^{2+} induces an increase in PL intensity,[39] and additional electron donation from PbS to the SWCNTs further increases the emission intensity (Figure S9). In contrast, Cd^{2+} causes a decrease in PL intensity,[39] whereas CdS promotes PL enhancement via electron transfer to the nanotubes (Figure S9); these opposing effects are likely the reason for the minimal PL change (~1%) observed for CdS-SWCNTs. For the Ag system, although Ag_2S nanoparticles can donate electrons to the SWCNTs (Figure S9) and increase PL intensity, this contribution is outweighed by ion-induced quenching,[40] leading to an overall decrease in PL intensity. This behaviour is further supported by the intrinsic sensitivity of Ag_2S to non-radiative pathways (Ag^+-trapped hole recombination), which are exacerbated when electronic coupling between the NP and the SWCNT is weak.[41-43]

For the in-situ method, fewer free metal ions remain because the precursors preferentially nucleate into nanoparticles on the DNA–SWCNT template, leading to multiple nanoparticles per nanotube. This creates numerous electronically coupled interfaces, increasing electron transfer from the NPs to the SWCNTs, stronger peak shift, and greater effect on the CNT PL emission: an increase of 14-17% was observed for all three NPs (Figure 3b).[44,45] The strong coupling achieved through direct seeding is particularly important for Ag_2S, whose band alignment sits near a critical threshold where small changes in distance and coupling determine whether electron injection or hole extraction dominates. Ag_2S known susceptibility to surface-mediated quenching, means that only in the in-situ configuration—where many NPs make intimate

contact with the SWCNT—does electron transfer outweigh ion-induced quenching. Conversely, CdS and PbS exhibit robust electron-donor behaviour across different surface environments, with CdS demonstrating field- and surface-dependent charge-transfer signatures[46,47] and PbS/CdS systems showing strong electron-transfer contributions even in assembled films,[48] explaining why they produce PL enhancement in both synthesis routes. Collectively, these results indicate that the distinct PL behaviours arise from a convergence of factors: ion-specific interactions with DNA, nanoparticle number and proximity, and the band-alignment-driven balance between quenching and electron-injection pathways.

We further observed PL peak shifting for the different nanohybrids and methods. Nanohybrids prepared via DNA hybridisation exhibit more varied behaviour, with PbS showing a blue shift while CdS and Ag_2S display red shifts. The blue shift observed for PbS may reflect stronger quantum confinement effects or changes in surface passivation,[49] while the larger shift observed for Ag_2S likely reflects the strong sensitivity of its emission to surface states and interfacial interactions within the CNT environment.[50] In contrast, the in-situ seeding methodology induces a distinct red shift in the PL emission across all the nanohybrids, indicative of bandgap renormalisation affecting both absorption and emission in these heterostructures.[50-51] A clearer indication of the peak shifting observed, and a comparison between the two methods are shown in Figure S10.

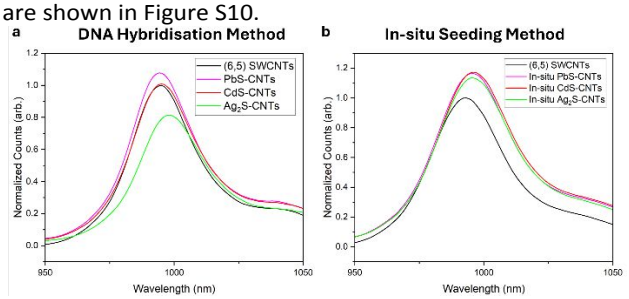

Figure 3: Steady-state photoluminescence characterization of SWCNT- based hybrids (under 575 nm excitation) obtained via the (a) DNA hybridisation and (b) in-situ methods. Full representative spectra are shown in Figure S11.

In conclusion, we investigated two distinct DNA-mediated functionalisation routes for the assembly of PbS, CdS, and Ag_2S NPs onto SWCNTs: via DNA hybridisation and in-situ seeding of cation precursors. AFM imaging demonstrated a clear distinction in the NPS density on CNTs obtained from the two strategies. Spectroscopic analysis revealed the impact on the optoelectronic properties of the hybrids. Our results showcase DNA templating as a valuable strategy to engineer 0D-1D heterostructures, providing design principles to modulate the local density environment towards (potential) programmable electronic coupling tunability. The application of this approach to different low-dimensional optoelectronic systems opens opportunities for the construction of nanoscale photodetectors, biosensors, and optoelectronic devices.[52]

Conflicts of interest

There are no conflicts to declare.

Data availability

All data used in this study are available in the published article and in the supplementary information (SI). SI: detailed experimental procedures and further characterization data.

Notes and references

1 P. Liu, S.-E. Yang, Y. Chen, Y. Ma, S. Liu, X. Fang, F. Fan and J. Han, Ceram. Int., 2020, 46, 19655–19663.
2 M. S. Dresselhaus, G. Dresselhaus and P. Avouris, Eds., Carbon Nanotubes, Springer Berlin Heidelberg, Berlin, Heidelberg, 2001, vol. 80.
3 P. Avouris, Z. Chen and V. Perebeinos, Nat. Nanotechnol., 2007, 2, 605–615.
4 A. López-Moreno, J. Villalva and E. M. Pérez, Chem. Soc. Rev., 2022, 51, 9433–9444.
5 Y. Li, Z. Hu, Q. Guo, J. Li, S. Liu, X. Xie, X. Zhang, L. Kang and Q. Li, Chem. Soc. Rev., 2025, 54, 5619–5656.
6 D. Eder, Chem. Rev., 2010, 110, 1348–1385.
7 N. Sultana, H. M. Dewey, A. G. Arellano and J. Budhathoki-Uprety, Chem. Mater., 2024, 36, 4034–4053.
8 G. A. Rance and A. N. Khlobystov, in Comprehensive Nanoscience and Nanotechnology, Elsevier, 2019, pp. 219–236.
9 M. Richter, T. Heumüller, G. J. Matt, W. Heiss and C. J. Brabec, Adv. Energy Mater., 2017, 7, 1601574.
10 S. Banerjee and S. S. Wong, Nano Lett., 2002, 2, 195–200.
11 J. M. Haremza, M. A. Hahn, T. D. Krauss, S. Chen and J. Calcines, Nano Lett., 2002, 2, 1253–1258.
12 S. Chaudhary, J. H. Kim, K. V. Singh and M. Ozkan, Nano Lett., 2004, 4, 2415–2419.
13 W. Yang, X. Wang, F. Yang, C. Yang and X. Yang, Adv. Mater., 2008, 20, 2579–2587.
14 R. J. Chen, Y. Zhang, D. Wang and H. Dai, J. Am. Chem. Soc., 2001, 123, 3838–3839.
15 X. L. Li, Y. Q. Liu, L. Fu, L. C. Cao, D. C. Wei and Y. Wang, Adv. Funct. Mater., 2006, 16, 2431–2437.
16 J. Zhao, H. Park, J. Han and J. P. Lu, J. Phys. Chem. B, 2004, 108, 4227–4230.
17 X. Li, Y. Jia and A. Cao, ACS Nano, 2010, 4, 506–512.
18 J. Schornbaum, B. Winter, S. P. Schießl, B. Butz, E. Spiecker and J. Zaumseil, Chem. Mater., 2013, 25, 2663–2669.
19 V. Pérez-Luna, S. Oros-Ruiz, E. Pérez and M. Quintana, Phys. Status Solidi B, 2017, 254, 1700197.
20 M. Zheng, A. Jagota, E. D. Semke, B. A. Diner, R. S. Mclean, S. R. Lustig, R. E. Richardson and N. G. Tassi, Nat. Mater., 2003, 2, 338–342.
21 A. Attanzio, A. Sapelkin, F. Gesuele, A. Van Der Zande, W. P. Gillin, M. Zheng and M. Palma, Small, 2017, 13, 1603042.
22 M. Freeley, A. Attanzio, A. Cecconello, G. Amoroso, P. Clement, G. Fernandez, F. Gesuele and M. Palma, Adv. Sci., 2018, 5, 1800596.
23 Z. Mengrani, W. Hong and M. Palma, ACS Nanosci. Au, 2024, 4, 391–398.
24 L. Dong, T. Hollis, B. A. Connolly, N. G. Wright, B. R. Horrocks and A. Houlton, Adv. Mater., 2007, 19, 1748–1751.

25 Q. Ye, X. Xu, A. Paghi, T. Bamford, B. R. Horrocks, A. Houlton, G. Barillaro, S. Dimitrov and M. Palma, Adv. Funct. Mater., 2021, 31, 2105719.
26 K. Chen, H. Miao, S. Dimitrov and M. Palma, Adv. Funct. Mater., 2025, 2502140.
27 K. Chen, H. Miao, W. Hong and M. Palma, Adv. Funct. Mater., 2025, e19712
28 D. Smith and G. Tikhomirov, ACS Appl. Opt. Mater., 2025, 3, 569–574.
29 J. Anastassopoulou, J. Mol. Struct., 2003, 651–653, 19–26.
30 N. T. K. Thanh, N. Maclean and S. Mahiddine, Chem. Rev., 2014, 114, 7610–7630.
31 O. A. Dyatlova, J. Gomis-Bresco, E. Malic, H. Telg, J. Maultzsch, G. Zhong, J. Geng and U. Woggon, Phys. Rev. B, 2012, 85, 245449.
32 W. Zhou, J. Vavro, N. M. Nemes, J. E. Fischer, F. Borondics, K. Kamarás and D. B. Tanner, Phys. Rev. B, 2005, 71, 205423.
33 A. Dzienia, D. Just and D. Janas, Nanoscale, 2023, 15, 9510–9524.
34 M. J. O'Connell, E. E. Eibergen and S. K. Doorn, Nat. Mater., 2005, 4, 412–418.
35 Y. Murakami and S. Maruyama, Phys. Rev. B, 2009, 79, 155445.
36 R. B. Weisman and J. Kono, in World Scientific Series on Carbon Nanoscience, World Scientific, 2019, vol. 10, pp. 1–43.
37 S. Suzuki and H. Hibino, Carbon, 2011, 49, 2264–2272.
38 I. O. Maciel, N. Anderson, M. A. Pimenta, A. Hartschuh, H. Qian, M. Terrones, H. Terrones, J. Campos-Delgado, A. M. Rao, L. Novotny and A. Jorio, Nat. Mater., 2008, 7, 878–883.
39 X. Liu, Y. Wang, J. Li and Z. Zhang, ACS Appl. Mater. Interfaces, 2011, 3, 3399–3405.
40 H. Liu, R. Guo, L. Li, Y. Wen, L. Wang, J. Yan and G. Liu, *ACS Appl. Nano Mater.*, 2025, **8**, 13719–13728
41 L. Du, W. Xiong, W. K. Chan and D. L. Phillips, Nanophotonics, 2018, 9, 4689–4701.
42 J. W. De Wit, I. Zabala-Gutierrez, R. Marin, A. Zhakeyev, S. Melle, O. G. Calderon, J. Marques-Hueso, D. Jaque, J. Rubio-Retama and A. Meijerink, J. Phys. Chem. Lett., 2024, 15, 8420–8426.
43 I. Grevtseva, O. Ovchinnikov, M. Smirnov, T. Kondratenko, A. Hussein, N. Egorov and E. Vozgorkova, J. Nanoparticle Res., 2023, 25, 118.
44 R. Chambard, J. C. Moreno-López, P. Hermet, Y. Sato, K. Suenaga, T. Pichler, B. Jousselme, R. Aznar, J.-L. Bantignies, N. Izard and L. Alvarez, Carbon, 2022, 186, 423–430.
45 W. Hong, B. Lambert, Z. Mengrani, L. Cognet and M. Palma, Small, 2025, e05186.
46 M. S. Mehata, Sci. Rep., 2015, 5, 12056.
47 M. K. Mahato, S. Roy and E. Prasad, J. Phys. Chem. C, 2024, 128, 12503–12510.
48 D. Pluta, R. T. Graf, D. Dorfs and N. C. Bigall, Phys. Chem. Chem. Phys., 2024, 26, 25828–25836.
49 J. Gao, W. Gomulya and M. A. Loi, Chem. Phys., 2013, 413, 35–38.
50 Y. Ohno, S. Iwasaki, Y. Murakami, S. Kishimoto, S. Maruyama and T. Mizutani, Phys. Status Solidi B, 2007, 244, 4002–4005.
51 C. A. Silvera-Batista, R. K. Wang, P. Weinberg and K. J. Ziegler, Phys. Chem. Chem. Phys., 2010, 12, 6990.
52 J. Z. Wu and M. Gong, Adv. Photonics Res., 2021, 2, 2100015.

View Article Online
DOI: 10.1039/D6CC02075E

View Article Online
DOI: 10.1039/D6CC02075E

Data availability

All data used in this study are available in the published article and in the supplementary information (SI). SI: detailed experimental procedures and further characterization data.